

Distorted-wave Born approximation and coupled channel analyses of low-energy polarized proton scattering on ^{24}Mg

R. M. Lombard and J. L. Escudé

Département de Physique Nucléaire, CEN Saclay, BP 2, 91190 Gif-sur-Yvette, France

M. Soyeur*

Service de Physique Théorique, CEN Saclay, BP 2, 91190 Gif-sur-Yvette, France.

(Received 12 January 1978)

Distorted-wave Born-approximation and coupled channel analyses of differential cross sections and analyzing powers have been performed for inelastic polarized proton-scattering data measured at an incident proton energy of 20.3 MeV. Collective and microscopic models have been used to describe the low-lying states of ^{24}Mg . The results obtained for the cross sections and analyzing powers with the rotational model description are in reasonably good agreement with the data. The distorted-wave Born-approximation analysis using shell-model wave functions gives satisfactory fits to the shape of the cross sections for some levels but very serious disagreements for the analyzing powers of almost all states, suggesting the need to include higher-order effects.

[NUCLEAR REACTIONS $^{24}\text{Mg}(p,p')$, $E=20.3$ MeV; calculated $\sigma(\theta)$ and analyzing power for 10 levels; macroscopic and microscopic DWBA calculations.]

I. INTRODUCTION

^{24}Mg has been extensively studied both theoretically and experimentally. Its spectrum shows a rotational band structure characteristic of a deformed nucleus. Two rotational bands should be distinguished: the ground state $K=0$ band and the excited $K=2$ band starting with the 2_2^+ state at 4.24 MeV. We denote with a lower index 1 the levels of the $K=0$ band (0_1^+ , 2_1^+ , 4_1^+ , ...) and with a lower index 2 the levels of the $K=2$ band (2_2^+ , 3_2^+ , 4_2^+ , ...). These rotational levels have been described by collective and microscopic models. In this second approach, recent extensive shell-model calculations^{1,2} succeeded in reproducing the collective nature of the rotational states insofar as they give large $B(E2)$ values (in agreement with the experimental data if one uses an effective charge of $0.5e$) for transitions within both the ground-state band and the excited band. One should note, however, that the cross band $E2$ transitions are usually overestimated by those calculations.

This paper deals with the analysis of 20.3 MeV polarized proton-scattering data on ^{24}Mg measured at the Saclay AVF cyclotron.³ The data consist of absolute cross sections and analyzing powers. The final states excited in this experiment are the 2_1^+ (1.37 MeV), 4_1^+ (4.12 MeV), and 6_1^+ (8.12 MeV) states of the ground-state rotational band, the 2_2^+ (4.24 MeV), 3_2^+ (5.23 MeV), and 4_2^+ (6.01 MeV) states of the excited band, the 0^+ state at 6.44 MeV, and the two 2^+ states at 7.35 and 8.65 MeV. The differential cross sections and analyzing powers

were measured from 20° to 160° . The experiment with a polarized beam gave only relative cross sections; the absolute values have been determined by an unpolarized beam measurement.

The analysis of those inelastic-scattering data do not give direct access to the detailed structure of the nuclear states as the reaction mechanism is not precisely known. Consequently, the aim of this paper will be twofold. For the collective model, effective deformation parameters will be deduced by distorted-wave Born approximation (DWBA) and coupled channel analyses (CC) and compared to values obtained in preceding experiments and with other probes. For the microscopic model, the DWBA analyses of the cross sections and analyzing powers will reflect the properties and uncertainties of the shell-model wave functions and of the distorted-wave Born approximation. In an attempt to disentangle both effects, the (pp') data will be analyzed with two sets of shell-model wave functions calculated in the same valence space and differing only in the choice of the effective interaction. It will be seen that even though this restricted difference in the shell-model wave functions may induce important differences in the cross sections and analyzing powers, the shortcomings of the DWBA approach are strongly suggested by the analyses of some of the data. This is in agreement with a recent paper⁴ showing the importance of two-step processes including the multipole giant resonance effects in the cross section analysis for the 3_2^+ at similar energies. In Sec. II, we describe the input of the

DWBA calculations, the nuclear wave functions used in the microscopic model analysis, and the coupled channel calculations. The numerical results for the cross sections and analyzing powers are shown and discussed in Sec. III and some general remarks on these results are given in Sec. IV.

II. DWBA AND COUPLED CHANNEL ANALYSES

The differential cross sections and analyzing powers were calculated in the distorted-wave Born approximation using macroscopic and microscopic models for all the levels mentioned in the Introduction.

Coupled channel calculations were performed for the 0_1^+ (g.s.), 2_1^+ (1.37 MeV), 4_1^+ (4.12 MeV), and 6_1^+ (8.12 MeV) states of the $K=0$ band (including the 8_1^+ state) within the symmetric rotational model and for the 0_1^+ (g.s.), 2_1^+ (1.37 MeV), 4_1^+ (4.12 MeV), 6_1^+ (8.12 MeV), 2_2^+ (4.24 MeV), 3_2^+ (5.23 MeV), and 4_2^+ (6.01 MeV) states of the $K=0$ and $K=2$ bands using the asymmetric rotational model.

A. DWBA analyses

Collective model: This analysis was carried out with the code written by Sherif. It includes the full Thomas term for the spin-orbit potential. The form factor is taken to be the deformation parameter β times the radial derivative of the optical potential. The entire optical potential is deformed in all calculations. The code allows us to use a spin-orbit term with a deformation different from that of the central and imaginary potentials; taking $\beta_{so} = 1.6\beta_L$ generally improves the predictions for the analyzing powers. The values of the parameters β_L entering the DWBA calculations are given in the first column of Table I(a).

Microscopic model: The calculations were performed in the antisymmetrized microscopic distorted-wave Born approximation using the code DWBA 74 written by Schaeffer and Raynal.

In this approximation the transition amplitude between the ground state and the final level is

$$T_{fi} = \frac{m(kk')^{1/2}}{(2\pi)^3} \langle \chi_{k'\sigma'}^- \Phi_f | V_{BF} | \chi_{k\sigma}^+ \Phi_i \rangle,$$

TABLE I. Deformation parameters β_L obtained in the DWBA analysis (a) and coupled channel (CC) analyses (b) compared to values extracted from other experiments. T refers to triaxial rotor model and S to symmetric rotor model.

Energy (MeV)	J^π	(a) β_L (DWBA)								
		(p,p')	(p,p') (Ref. 5)	(p,p') (Ref. 6)	(p,p') (Refs. 7 and 8)	(p,p') (Ref. 9)	(n,n') (Ref. 10)	(³ He, ³ He) (Ref. 11)	(α , α') (Ref. 12)	
		20.3 MeV this work	17 MeV	30 MeV	40 MeV	49.5 MeV S T	14 MeV	29 MeV	43 MeV	
1.37	2 ⁺	0.52	0.52	0.58	0.475	0.49	0.37	0.62	0.40	0.55-0.66
4.12	4 ⁺	0.12					$\gamma = 32^\circ$		0.10	
4.24	2 ⁺	0.16							0.2	
6.01	4 ⁺	0.27								
7.35	2 ⁺	0.14	0.15							
8.65	2 ⁺	0.10								
		(b)								
Experiment		Coupled states			β_2	β_4	β_6	γ		
17.5 MeV (p,p') (Ref. 24)		S(β_2, β_4)			0.47	-0.05				
20.3 MeV (p,p')		S($\beta_2, \beta_4, \beta_6$)			0.47	-0.056	+0.054			
This work		T($\beta_2, \beta_4, \beta_6, \gamma$)			0.47	-0.060	+0.054	21°		
22.5-28.5 MeV (p,p') (Ref. 4)		T(β_2, γ)			0.50-0.56			20°-22°		
30.5 MeV (p,p') (Ref. 6)		T(β_2, γ)			0.50			23°		
40 MeV (p,p') (Refs. 7 and 8)		S(β_2)			0.47					
49.5 MeV (p,p') (Ref. 9)		S(β_2)			0.49					
14 MeV (n,n') (Ref. 10)		S(β_2)			0.53					
26 MeV (d,d') (Ref. 25)		S(β_2)			0.42					
17 MeV (α, α') (Ref. 26)		S(β_2, β_4)			0.40	0.05				
28.5 MeV (α, α') (Ref. 27)		T(β_2, γ)			0.34			35°		
104 MeV (α, α') (Ref. 28)		S(β_2, β_4)			0.39	-0.015				
187 MeV (e,e') (Ref. 29)		S(β_2)			0.51					
183-250 MeV (e,e') (Ref. 30)		S(β_2, β_4)			0.45	-0.06				

TABLE II. Optical-model parameters at 20.3 MeV proton energy.

	V (MeV)	r (fm)	a (fm)	W_i (MeV)	r_i (fm)	a_i (fm)	V_s (MeV)	r_s (fm)	a_s (fm)	r_c (fm)
Elastic scattering										
microscopic DWBA	43.52	1.25	0.59	6.34	1.26	0.517	4.77	1.03	0.35	1.20
Inelastic scattering (cc)										
rotational S	48.62	1.15	0.67	7.69	1.37	0.28	4.6	0.94	0.40	1.20
Asym. rotational T	48.62	1.15	0.67	7.76	1.37	0.28	4.56	0.94	0.40	1.20

where χ^+ and χ^- are the ingoing and outgoing distorted-wave functions determined by an optical-model calculation, V_{BF} is an effective “bound-free” nucleon-nucleon interaction and Φ_i and Φ_f are the wave functions describing the initial and final states.

The antisymmetrization between incoming and bound particles is fully taken into account. The calculation is direct in the sense that no multistep process involving intermediate states is included.

The optical-model parameters have been determined with the code MAGALI written by Raynal; the parameters used in our calculations are given in the first row of Table II.

The outgoing channel has been computed taking into account the energy dependence of the optical potential well. A search consistent with the Julich⁴ analysis taking the same geometrical parameters and spin-orbit potential gives well depths smoothly related to the Julich parameters. Moreover, using the (pp) data at 17.5 MeV from Crawley and Garvey⁵ and the systematics of Colombo *et al.*¹³ between 20 and 40 MeV, no evidence for a resonant or anomalous effect was found around 20 MeV.

The “bound-free” nucleon-nucleon interaction contains central, spin-orbit, and tensor terms with spin and isospin dependence. We have considered two nucleon-nucleon interactions, a force derived from the Hamada-Johnston potential¹⁴ on the one hand and the MSU force of Borysowicz *et al.*¹⁵ on the other hand. The latter is an effective interaction obtained by fitting with a sum of Yukawa forces the matrix elements of a G matrix computed from the Reid potential in an harmonic-oscillator basis. The strengths and ranges of the various terms obtained from a three-Yukawa fit to the original force (up to momenta of 2 fm^{-1}) are listed in Table III.

From the comparison of numerical results for cross sections obtained with both forces it turns out that for a given transition they differ essentially by a normalization factor. The cross sections given by the MSU force are usually 1.5 times larger than the Hamada-Johnston predictions for both direct and exchange terms. This effect was

already observed and discussed in the analysis of $^{15}\text{N}(pp')$ data between 20 and 30 MeV.¹⁶ Therefore, and as no marked change in the analyzing powers is induced by the difference in the spin-orbit interaction of the two forces, the results obtained with the MSU force only will be presented in this paper.

To describe the low-lying states of ^{24}Mg , we take the shell-model wave functions of Soyeur¹ and Wildenthal² obtained by diagonalizing an effective Hamiltonian in the full ($2s-1d$) shell space for eight valence nucleons. They both use the single-particle energies given by the ^{17}O spectrum. The calculations differ by the choice of the effective interaction.

Soyeur takes the effective nucleon-nucleon interaction derived from a separable potential by Kahana *et al.*,¹⁷ while Wildenthal uses the fitted interaction of Chung and Wildenthal.¹⁸

The energy spectra and electromagnetic $E2$ transition rates calculated with those wave functions are given in Fig. 1 and Table IV, respectively. The general features of the calculations are that the energy spectrum is roughly reproduced for the first excited states and that the cross band $E2$ transitions are generally too large while the $B(E2)$ values within the $K=0$ and $K=2$ bands are in excellent agreement with the experimental data (one uses an effective charge of $0.5e$). For the spectrum calculated with the Kahana *et al.* effective interaction, it seems, however, that the first levels of the $K=2$ band come systematically too low in energy.

TABLE III. Parameters of the three Yukawa potentials used to describe the “bound-free” nucleon-nucleon interaction.

Range (fm)	Depths (MeV)					
	Triplet even	Singlet even	LS even	LS odd	Tensor even	Tensor odd
0.3	8491	5774	-1650	-5938.8	0	0
0.5	-2656	-1785.6	-0.20	166.5	-476.4	151.38
0.86	0	0	0	0	-4.01	0.332

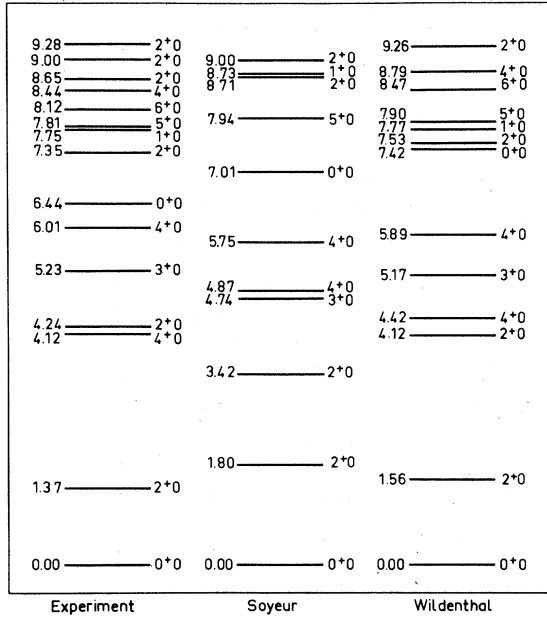


FIG. 1. Energy spectrum of ^{24}Mg ($T=0$, positive parity states). From left to right, experimental spectrum and theoretical spectra corresponding to Soyeur's and Wildenthal's wave functions.

The wave functions enter the calculations through the matrix elements $Z_{j_1 j_2}^{JT}$ of the particle-hole excitation operators. Harmonic oscillator and various Woods-Saxon wave functions were used to describe the single-particle states. The results presented in this paper are obtained with a Woods-Saxon potential corresponding to the following binding energies: for the protons $v_{5/2}=12.89$ MeV, $v_{1/2}=11.44$ MeV, and $v_{3/2}=7.57$ MeV, for the neutrons $v_{5/2}=16.54$ MeV, $v_{1/2}=15.09$ MeV, and $v_{3/2}=11.22$ MeV.

The spectroscopic amplitudes $Z_{j_1 j_2}^{JT}$ were normalized by a factor Λ to give the correct absolute values for the cross sections. This factor Λ is related to the isoscalar polarization charge e_0 [which gives an effective charge of $(1+e_0)$ for the proton and e_0 for the neutron] by $\Lambda = 1 + 2e_0$. As we consider $T=0$ transitions, the isoscalar polarization charge only will contribute. The values of Λ used for each transition are given in Table V. The cross sections shown in the figures will be normalized by those factors and consequently only the shape of the cross sections reflects the agreement or disagreement between theory and experiment.

Finally, for the states for which the real form factor is collective, we have added a complex form factor. While the real part results from a microscopic calculation, the imaginary part is macro-

TABLE IV. Experimental and theoretical $B(E2)$ values for the low-lying states of ^{24}Mg . The calculated shell-model values are obtained using an effective charge of $0.5e$ for protons and neutrons.

Initial state	Final state	Experiment (Ref. 19)	Soyeur (Ref. 1)	Wildenthal (Ref. 2)
		($e^2 \text{fm}^4$)	($e^2 \text{fm}^4$)	($e^2 \text{fm}^4$)

$B(E2)$ values within the ground state band

2 ⁺	1.37 MeV 0 ⁺	0.00 MeV	84.3 ± 2.5	83.2	103
4 ⁺	4.12 MeV 2 ⁺	1.37 MeV	95^{+21}_{-16}	98.8	130
6 ⁺	8.12 MeV 4 ⁺	4.12 MeV	140^{+148}_{-25}	92.3	121

$B(E2)$ values within the excited $K=2$ band

3 ⁺	5.23 MeV 2 ⁺	4.24 MeV	127 ± 21	143.9	178
			(Ref. 20)		
4 ⁺	6.01 MeV 2 ⁺	4.24 MeV	66^{+16}_{-12}	35.9	54.6
5 ⁺	7.81 MeV 3 ⁺	5.23 MeV	148^{+25}_{-21}	56.6	75
5 ⁺	7.81 MeV 4 ⁺	6.01 MeV	62^{+21}_{-12}	71.5	85.4

$B(E2)$ values for cross band transitions

2 ⁺	4.24 MeV 0 ⁺	0.00 MeV	$5.7^{+1.2}_{-0.8}$	5.2	11.2
2 ⁺	4.24 MeV 2 ⁺	1.37 MeV	$8.6^{+2.5}_{-1.6}$	38.8	20.2
3 ⁺	5.23 MeV 2 ⁺	1.37 MeV	8.6 ± 1.2	8.7	17.8
4 ⁺	6.01 MeV 2 ⁺	1.37 MeV	4.1 ± 1.2	13.0	12.4
4 ⁺	6.01 MeV 4 ⁺	4.12 MeV	<4 (Ref. 20)	16.7	13.3

$B(E2)$ values involving the 0⁺ state at 6.44 MeV

0 ⁺	6.44 MeV 2 ⁺	1.37 MeV	1.9 ± 0.3	2.2	0.10
0 ⁺	6.44 MeV 2 ⁺	4.24 MeV	22 ± 7	7.3	21.3

scopic. Following Terrien *et al.*,²¹ Satchler,²² and various other authors, it is taken to be the derivative of the imaginary part of the optical potential times the collective deformation parameter β . As the real form factors were normalized to the ab-

TABLE V. Normalizing factors Λ used in the microscopic DWBA analysis with Soyeur's and Wildenthal's shell-model wave functions.

Level	Spin	$\Lambda = (\sigma_{\text{exp}}/\sigma_{\text{th}})^{1/2}$	
		Soyeur	Wildenthal
1.37	2 ⁺	1.62	2
4.12	4 ⁺	4.65	2.74
4.24	2 ⁺	1.73	1.73
5.23	3 ⁺	10	8.12
6.01	4 ⁺	2	4.46
6.44	0 ⁺	1.79	1.82
7.35	2 ⁺	1.96	1.48
8.65	2 ⁺		4.47

solute values of the cross sections, the addition of an imaginary form factor will contribute very little to the total cross sections.

B. Coupled channel analyses

The coupled channel calculations were performed with the code ECIS written by Raynal. As suggested by various preceding calculations,²³ the spin-orbit deformation was increased by a factor of 1.9 in order to improve the fits to the analyzing powers. Both symmetric and asymmetric rotational models were used to analyze the data. The optical-potential parameters are given in the second row of Table II for the symmetric rotational model and in the third row of Table II for the asymmetric rotational model.

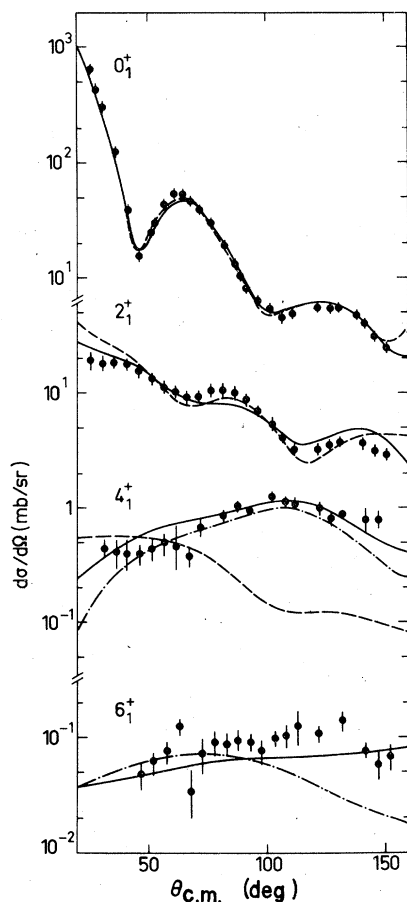


FIG. 2. Experimental and theoretical differential cross sections for the ground-state rotational band levels, i.e., the ground state (0_1^+), 2_1^+ state (1.37 MeV), 4_1^+ state (4.12 MeV), and 6_1^+ state (8.12 MeV) using the symmetric rotational model. The dashed lines refer to DWBA analyses with $\beta = 0.52$ (2_1^+) and $\beta = 0.12$ (4_1^+) and the solid and dot-dashed lines to coupled channel calculations using $\beta_2 = 0.47$, $\beta_4 = -0.056$, and $\beta_6 = +0.054$ (solid line) or $\beta_6 = -0.046$ (dot-dashed line).

III. NUMERICAL RESULTS

A. Ground-state rotational band levels

Macroscopic analyses: The DWBA and coupled channel analyses using the macroscopic model are shown for the cross sections and analyzing powers of the levels of the $K=0$ band on Figs. 2–5. The DWBA calculations give good fits to the data for the ground state and for the 2_1^+ state with a deformation parameter $\beta = 0.52$. For the 4_1^+ state, except at forward angles, the fit to the cross section ($\beta = 0.12$) is extremely bad in the DWBA analysis;

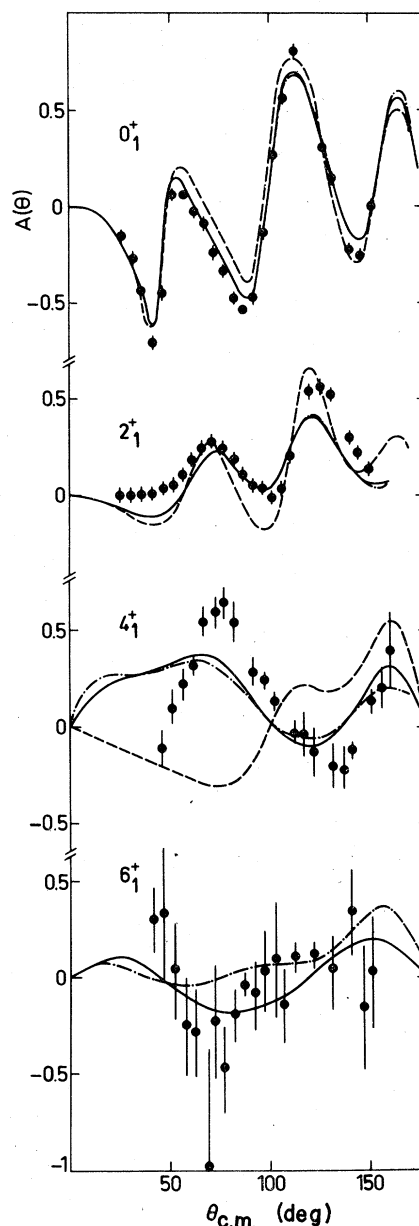


FIG. 3. Same as Fig. 2 for analyzing powers.

the calculated analyzing power has essentially nothing to do with the experimental points. This problem is cured by the coupled channel treatment using the symmetric rotational model. The 0_1^+ , 2_1^+ , and 4_1^+ cross sections and analyzing powers are very well reproduced for the values $\beta_2=0.47$ and $\beta_4=-0.056$. For the 6_1^+ state a positive β_6 deformation parameter of 0.054 is needed to fit the cross section. The search was also made for negative deformation and gave $\beta_6=-0.046$. The positive deformation is slightly favored by χ^2 criterion. We have checked that the coupling of the 8_1^+ state does not modify the determination of β_6 .

The value $\beta=0.52$ obtained by the DWBA analysis for the 2_1^+ state is in agreement with the values listed in Table I(a) extracted from various

proton-, neutron-, and α -scattering data analyzed in the distorted-wave Born approximation. A similar conclusion can be drawn from Table I(b) for the coupled channel treatment giving $\beta_2=0.47$ and $\beta_4=-0.056$ in the rotational symmetric (S) model. The value obtained for β_2 using α -scattering data is, however, a little bit smaller. The deformations β_2 and β_4 deduced in this work are in agreement with a previous analysis of inelastic electron scattering data.³⁰

Coupled channel calculations with a triaxially deformed potential (T) were also performed

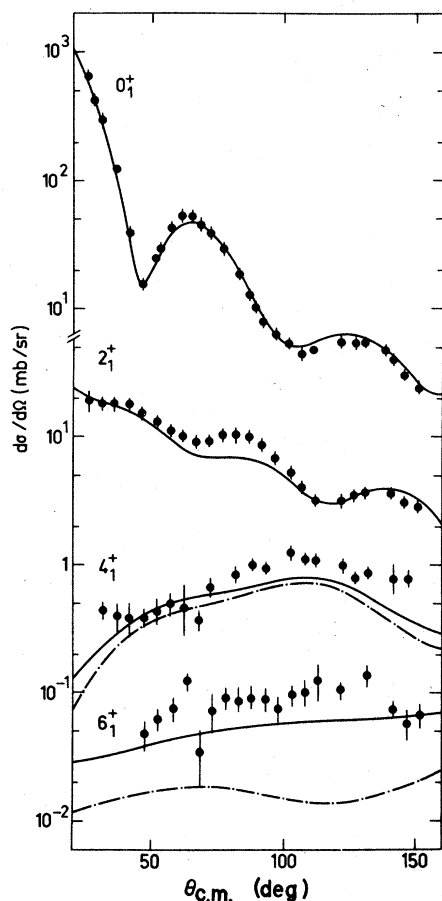


FIG. 4. Experimental and theoretical differential cross sections for the ground-state rotational band levels using the asymmetric rotational model in a coupled channel analysis involving the 0_1^+ , 2_1^+ , 4_1^+ , 6_1^+ , 2_2^+ , 3_2^+ , and 4_2^+ states. The values of the parameters are $\gamma=21^\circ 5'$, $\beta_2=0.47$, $\beta_4=-0.060$, and $\beta_6=0.054$ (solid line); we show for comparison the curves obtained for the 4_1^+ and 6_1^+ states with a β_2 deformation only, i.e., $\beta_4=\beta_6=0$ (dot-dashed line).

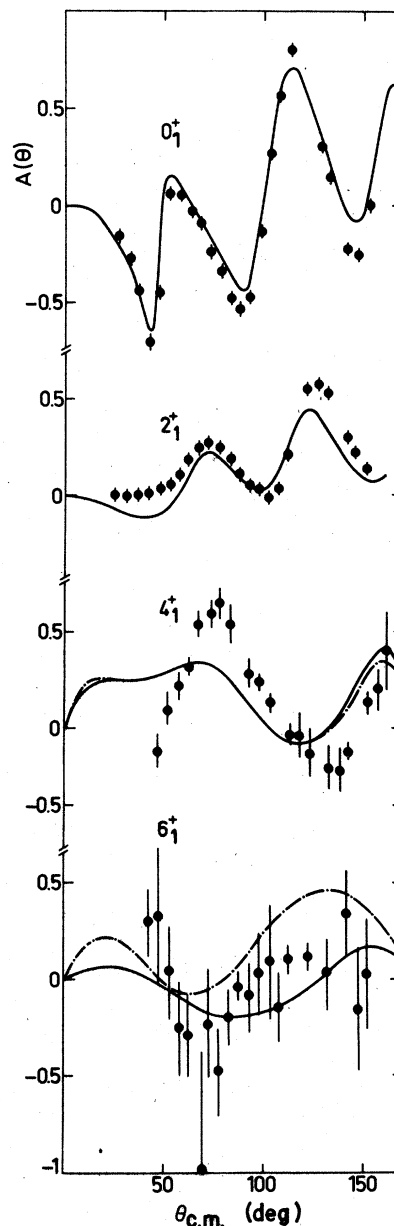


FIG. 5. Same as Fig. 4 for analyzing power.

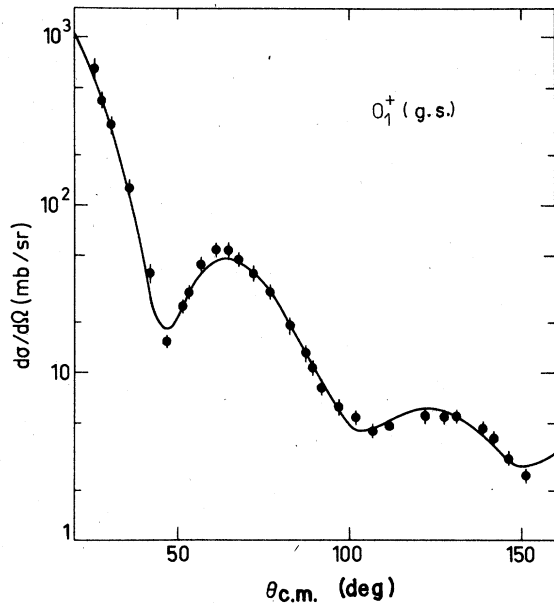


FIG. 6. Optical-model analysis of the elastic differential cross section.

coupling the 0_1^+ , 2_1^+ , 4_1^+ , 6_1^+ , 2_2^+ , 3_2^+ , and 4_2^+ states. The fit obtained for the $K=0$ band levels is reasonably good for values of $\beta_2=0.47$, $\beta_4=-0.060$, $\beta_6=0.054$, and $\gamma=21^\circ$. For the 4_1^+ and 6_1^+ states, we have quoted on Figs. 4 and 5 the cross sections and analyzing powers obtained with a β_2 deformation only. It can be seen from the figures that for the 6_1^+ state, nonzero β_4 and β_6 substantially improve the fit to the cross section.

Microscopic analysis: The microscopic DWBA analyses of the cross sections and analyzing powers using the shell-model wave functions of Soyeur (S) and Wildenthal (W) are given for the 2_1^+ and 4_1^+ states in Figs. 8–11. Figures 6 and 7 show the fit to the elastic data obtained with the code MAGALI.

For the 2_1^+ state, the differential cross section is quite well reproduced by both shell-model wave functions except for the plateau at forward angles. The normalization factor Λ of the order of 2 is in agreement with the corresponding effective charge in electromagnetic transition rates.

It is also clear from Fig. 8(b) that adding an imaginary form factor slightly improves the fit to the experimental cross section. Very similar results are obtained with the two wave functions.

The 4_1^+ cross section analyzed with shell-model wave functions shows the same behavior as the DWBA macroscopic model analysis. The calculated cross section is too low beyond 90° and a larger factor is needed to normalize the absolute cross section: $\Lambda=4.65$ for the Soyeur wave functions, $\Lambda=2.74$ for the Wildenthal wave functions. This and

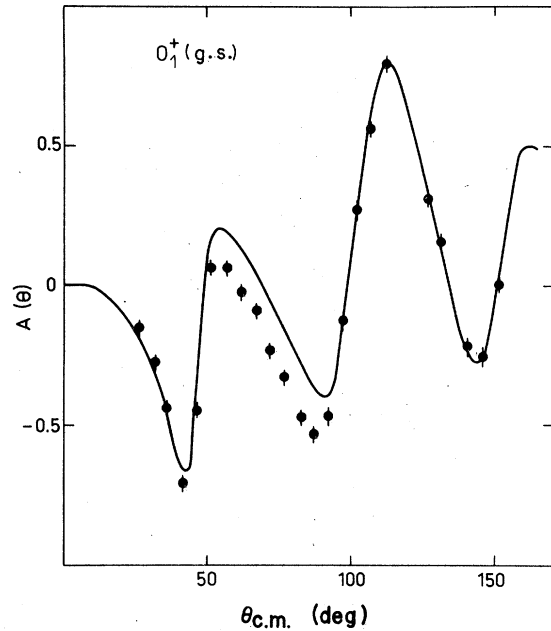


FIG. 7. Same as Fig. 6 for the analyzing power.

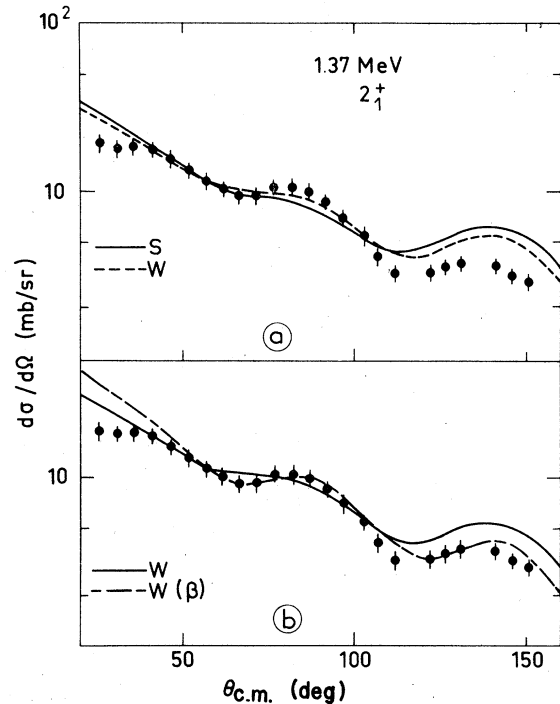


FIG. 8. Experimental and theoretical differential cross sections for the 2_1^+ state (1.37 MeV) obtained by a DWBA analysis using shell-model wave functions. Figure 8(a) shows a comparison of the Soyeur (solid line) and Wildenthal (dashed line) wave functions with $\Lambda=1.62$ and $\Lambda=2$, respectively. Figure 8(b) shows the effect of adding an imaginary form factor (dot-dashed line) with $\beta=0.52$ to the previous calculation (solid line) using Wildenthal's wave function.

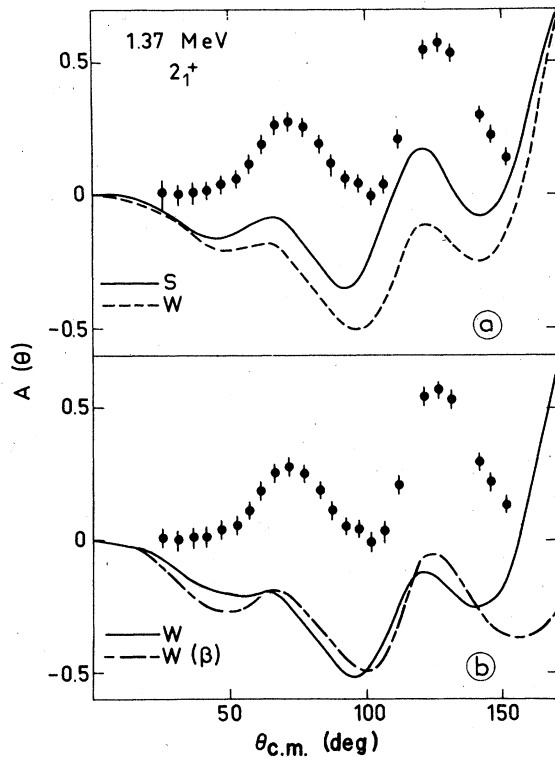


FIG. 9. Same as Fig. 8 for analyzing powers.

the complete lack of structure in the calculated cross sections suggest the importance of intermediate state contributions.

The analyzing powers for the 2_1^+ and 4_1^+ states are not at all reproduced by the microscopic DWBA calculations. For the 4_1^+ state, however, the discrepancy is reduced by the introduction of an imaginary form factor.

An interesting effect is observed for the 2_1^+ analyzing powers; there is a marked difference between the curves calculated with both wave functions. This suggests that analyzing powers are very sensitive observables and could test the detailed structure of the nuclear states if the reaction mechanism was fully understood.

B. Excited $K = 2$ rotational band levels

Macroscopic analyses: The DWBA and coupled channel analyses using the macroscopic model are shown for the cross sections and analyzing powers of the levels of the $K = 2$ band in Figs. 12 and 13, respectively.

The DWBA calculations reproduce the cross sections for the 2_2^+ and 4_2^+ states at small angles with $\beta = 0.16$ and $\beta = 0.27$. For the 2_2^+ , the calculation fails to give the correct behavior of the cross section for angles larger than 90° . The general

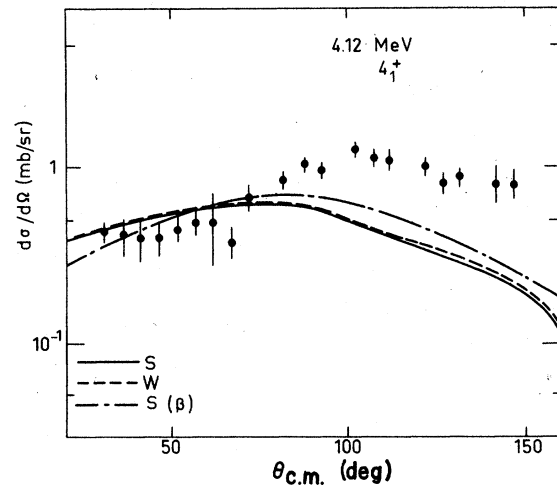


FIG. 10. Experimental and theoretical differential cross sections for the 4_1^+ state (4.12 MeV) obtained by a DWBA analysis using Soyeur's (solid line) and Wildenthal's (dashed line) shell-model wave functions with $\Lambda = 4.65$ and $\Lambda = 2.74$, respectively. The dot-dashed line shows the effect of adding an imaginary form factor ($\beta = 0.12$) with Soyeur's wave function.

shape of the analyzing powers for the 2_2^+ and 4_2^+ states are essentially given by the DWBA analysis but no detailed agreement is achieved.

The coupled channel approach has been used to analyze the 2_2^+ , 3_2^+ , and 4_2^+ cross sections and analyzing powers using the asymmetric rotational model and including the 0_1^+ , 2_1^+ , 4_1^+ , and 6_1^+ states in the calculations.

Results very similar to those of the DWBA analysis were obtained for the 2_2^+ state using $\beta_2 = 0.47$, $\beta_4 = -0.060$, $\beta_6 = +0.054$, and $\gamma = 21^\circ$. This value of γ is in agreement with the value determined in

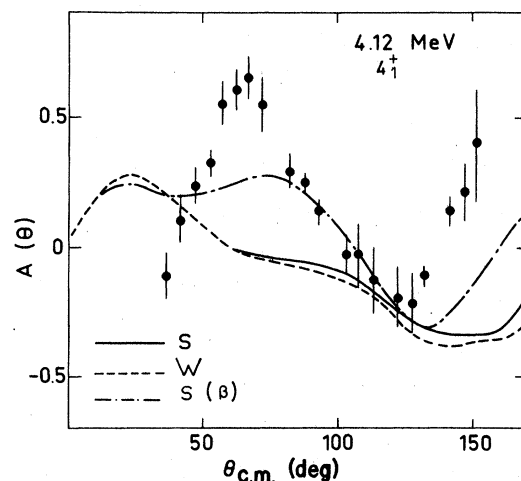


FIG. 11. Same as Fig. 10 for the analyzing powers.

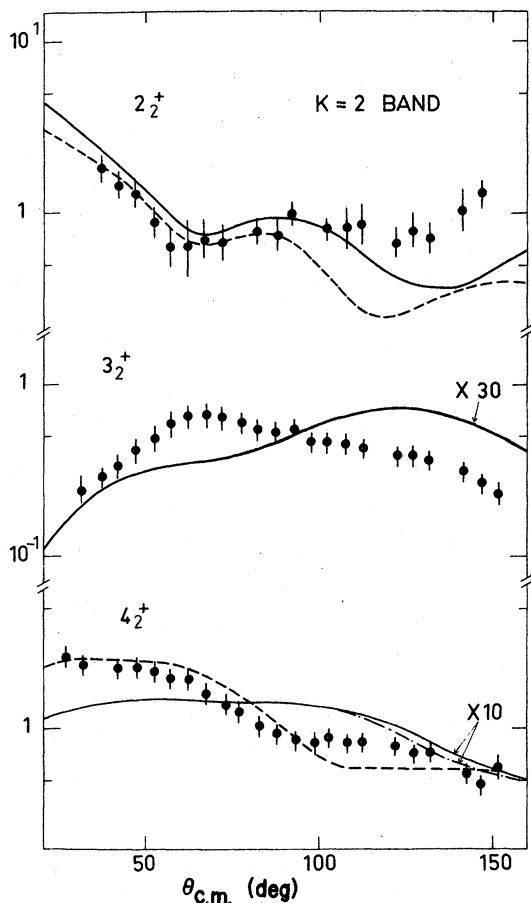


FIG. 12. Experimental and theoretical differential cross sections for the $K=2$ rotational band levels, i.e., the 2_2^+ state (4.24 MeV), the 3_2^+ state (5.23 MeV), and the 4_2^+ state (6.01 MeV). The dashed lines refer to DWBA analyses with $\beta=0.16$ (2_2^+) and $\beta=0.27$ (4_2^+) and the solid and dot-dashed lines to coupled channel calculations using $\gamma=21.5$, $\beta_2=0.47$, $\beta_4=-0.060$, $\beta_6=0.054$ (solid line), and $\beta_4=\beta_6=0$ (dot-dashed line).

Ref. 4 for similar proton energies.

The cross section for the 3_2^+ state is not given at all by this calculation: The absolute value is 30 times too small and the shape is not reproduced. The disagreement is less important for the analyzing power even though its detailed structure is clearly not obtained in this analysis. As can be seen from Figs. 12 and 13, nonzero values for β_4 and β_6 have essentially no effect on the cross section and analyzing power.

The strong underestimation of the 3_2^+ cross section within this model suggests that an important coupling is missing. Lovas *et al.*⁴ were able to improve this cross section by including the dipole and quadrupole giant resonances as doorway states through an exchange process. This is likely to be

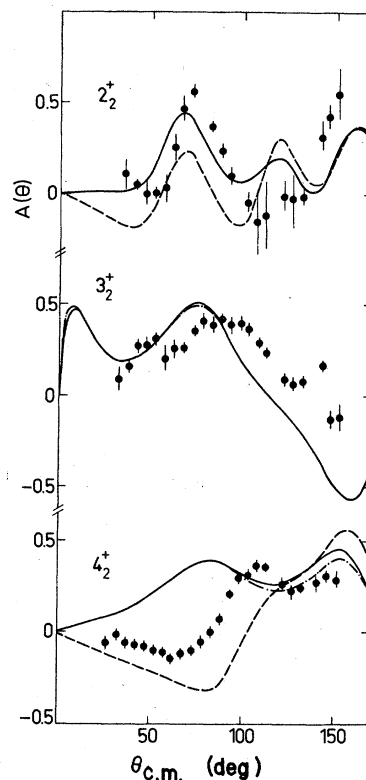


FIG. 13. Same as Fig. 12 for analyzing powers.

the most important coupling lacking in our calculation.

The situation for the 4_2^+ level is, however, different. Although the cross section is underestimated by an order of magnitude and is not reproduced by the triaxial model, the transition here is a natural

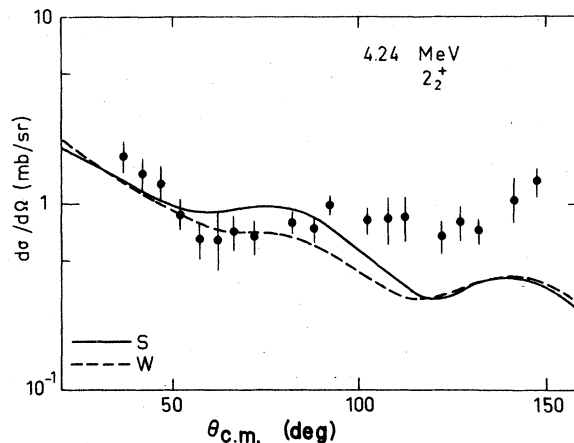


FIG. 14. Experimental and theoretical differential cross sections for the 2_2^+ state (4.24 MeV) obtained by a DWBA analysis using Soyeur's (solid line) and Wildenthal's (dashed line) shell-model wave functions with $\Lambda=1.73$ for both cases.

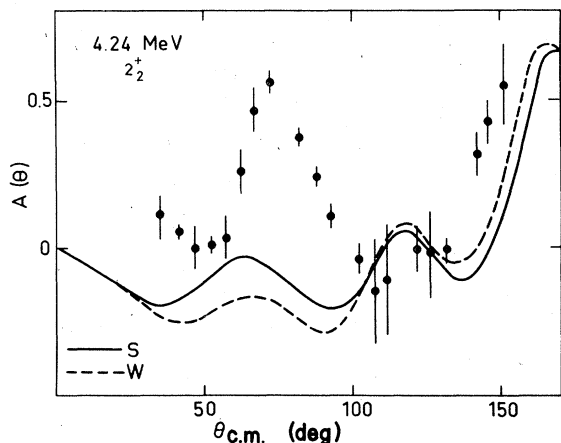


FIG. 15. Same as Fig. 14 for analyzing powers.

parity one, minimizing the relative importance of such doorway states. The ability of either macroscopic or microscopic DWBA calculations to fill the level in accordance with the experiment hints that the direct transition matrix element is underestimated by the asymmetric-rotor-model calculation.

Microscopic analyses: The microscopic DWBA analyses of the cross sections and analyzing powers using the shell-model wave functions of Soyeur and Wildenthal are given for the 2_2^+ , 3_2^+ , and 4_2^+ states of the $K=2$ band in Figs. 14–19.

The shape of the cross section for the 2_2^+ state at 4.24 MeV is not very well given by this analysis, while the overall normalization factor $\Lambda = 1.73$ for both wave functions is in agreement with what is needed for electromagnetic properties.

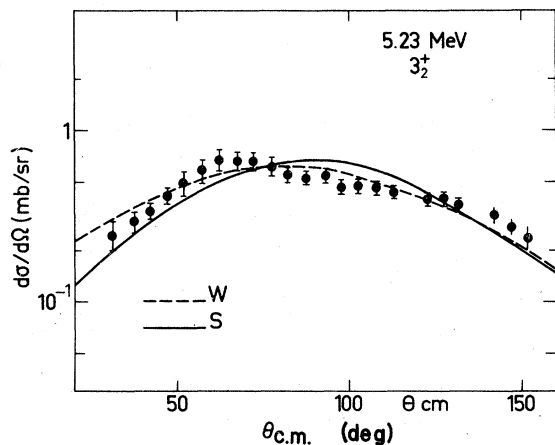


FIG. 16. Experimental and theoretical differential cross sections for the 3_2^+ state (5.23 MeV) obtained by a DWBA analysis using Soyeur's (solid line) and Wildenthal's (dashed line) shell-model wave functions with $\Lambda = 10$ and $\Lambda = 8.12$, respectively.

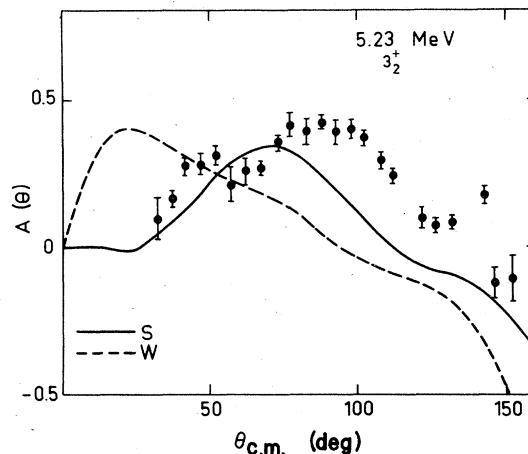


FIG. 17. Same as Fig. 16 for analyzing powers.

It is interesting to note that the shape of the predicted cross sections for the 2_2^+ state is in fact very similar to the shape of the 2_1^+ cross section while the experimental data are quite different at large angles. This may be understood if one looks at the $B(E2)$ values given in Table IV. In particular, the $E2$ cross band transition from the 2_2^+ to the 2_1^+ is too large, indicating that those two states are in some sense too much alike. Therefore, the similarity of the (pp') cross sections for the 2_1^+ and 2_2^+ states may simply reflect the shortcomings of the shell-model wave functions.

The shape of the 3_2^+ cross section is roughly

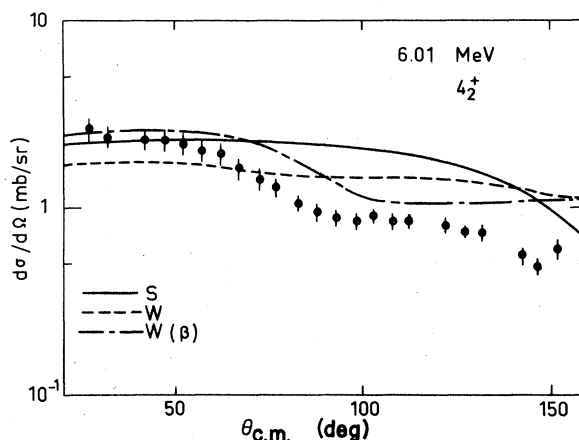


FIG. 18. Experimental and theoretical differential cross sections for the 4_2^+ state (6.01 MeV) obtained by a DWBA analysis using Soyeur's (solid line) and Wildenthal's (dashed line) shell-model wave functions with $\Lambda = 2$ and $\Lambda = 4.46$. The dot-dashed curve shows the effect of adding an imaginary form factor ($\beta = 0.27$) with Wildenthal's wave function.

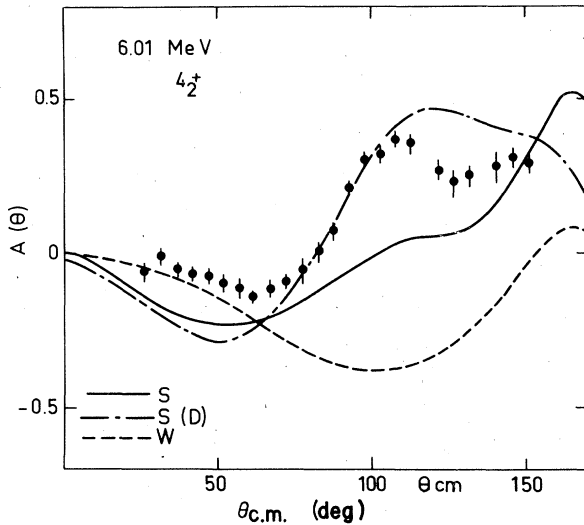


FIG. 19. Same as Fig. 18 for the analyzing powers. A dot-dashed curve indicates the direct term only calculated with Soyeur's wave function.

given by the DWBA analysis with shell-model wave functions even though there seems to be much more structure in the experimental points than in the calculated cross sections. The normalization, however, is not given at all by the calculation, as is to be expected from the macroscopic analysis. The values of Λ are 10 and 8.12 for Soyeur's and Wildenthal's wave functions, respectively, indicating that very important contributions to the cross section are missing in the analysis. The 4_2^+ cross section is not well given by the microscopic DWBA calculations. The shapes obtained with both wave functions are much too flat. This can be improved by adding an imaginary form factor but the behavior of the cross section at backward angles is still not reproduced. One should also remark that the normalization factors Λ are quite different for the two wave functions: $\Lambda = 2$ for Soyeur's and $\Lambda = 4.46$ for Wildenthal's wave functions.

The analyzing powers for the 2_2^+ , 3_2^+ , and 4_2^+ states are not even qualitatively reproduced by the microscopic DWBA analysis. The only interesting information that can be extracted from Figs. 15, 17, and 19, besides the fact that our analysis is clearly not correct for those states, is that the two wave functions lead to very different curves, reinforcing our previous remark about the sensitivity of the analyzing powers to the details of the nuclear wave functions. It is also interesting to remark that the direct term only gives quite a good fit to the analyzing power of the 4_2^+ state (Fig. 19).

C. Other levels: 0^+ (6.44 MeV), 2_3^+ (7.35 MeV), 2_4^+ (8.65 MeV).

Macroscopic Model: The DWBA analysis of the cross sections and analyzing powers for the 2_3^+ and 2_4^+ states calculated with the macroscopic model are shown in Figs. 20 and 21.

With $\beta = 0.14$ for the 2_3^+ state and $\beta = 0.10$ for the 2_4^+ state, the agreement between the calculated and measured cross sections and analyzing powers is very poor. This is not too surprising since the collective character of those two 2^+ states is not all established. Very little improvement is achieved by increasing the spin-orbit deformation ($\beta_{so} = 1.6\beta$).

Microscopic Model: The microscopic DWBA analyses of the cross sections and analyzing powers using Soyeur's and Wildenthal's shell-model wave functions are given for the 0^+ state at 6.44 MeV and for the 2^+ states at 7.35 and 8.65 MeV in Figs. 22–27. The Wildenthal wave functions only are used to analyze this last level.

For none of these three levels are the cross sections or analyzing powers reasonably well reproduced by the microscopic DWBA treatment. The structure of the cross sections is not given at all and the analyzing powers predicted by the analysis have almost nothing to do with the experimental curves. For the 0^+ and the 2_3^+ states, the normalization factors are quite reasonable: $\Lambda = 1.79$ and $\Lambda = 1.96$ for the Soyeur wave functions, $\Lambda = 1.82$ and $\Lambda = 1.48$ for the Wildenthal wave functions. For the 2_4^+ state, the normalization factor is larger, $\Lambda = 4.47$.

Again we would like to point out that important differences in the analyzing powers are obtained with the two sets of wave functions. This is also true to a lesser extent for the cross section of the 2_3^+ state.

IV. CONCLUSION

Detailed and constructive conclusions are very hard to draw from the results discussed in this paper. A few general remarks do nevertheless emerge from the calculations which can be summarized as follows.

The macroscopic model analyses give reasonable fits to the data in most cases for values of the deformation parameters in agreement with preceding determinations. Evidence for intermediate coupling is obtained for the 4_1^+ state of the $K=0$ band and for the 3_2^+ and 4_2^+ states of the $K=2$ band.

It is worthwhile to stress that the rather good agreement between the data and the asymmetric-rotor calculation does not mean that the ^{24}Mg is a rigid rotor. Recent Hartree-Fock calculations

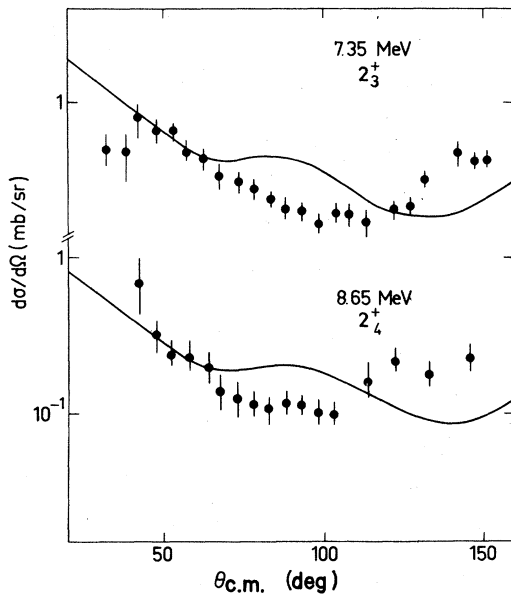


FIG. 20. Experimental and theoretical cross sections for the 2_3^+ state (7.35 MeV) and 2_4^+ state (8.65 MeV) obtained by a DWBA analysis using the rotational model ($\beta = 0.14$ for the 2_3^+ and $\beta = 0.10$ for the 2_4^+).

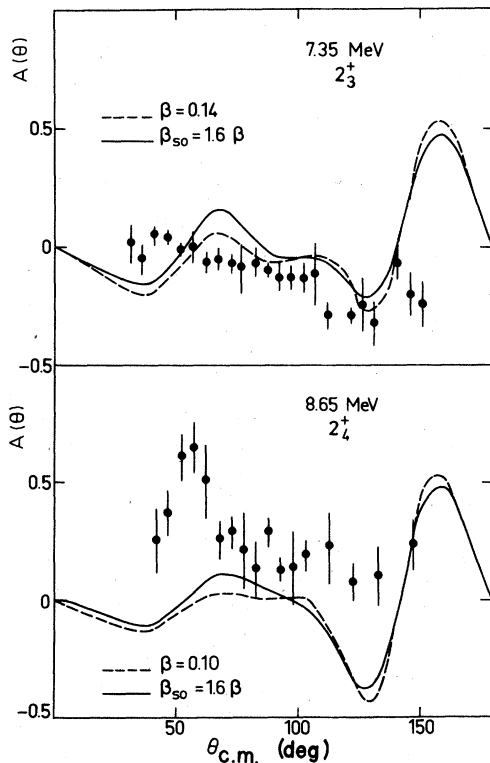


FIG. 21. Same as Fig. 20 for the analyzing powers (dashed line). The solid line shows the effect of an increased spin-orbit deformation $\beta_{so} = 1.6\beta$.

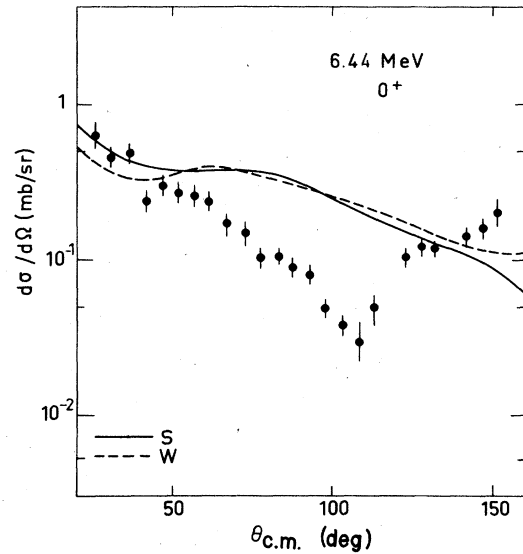


FIG. 22. Experimental and theoretical cross sections for the first excited 0^+ state (6.44 MeV) obtained by a DWBA analysis using Soyeur's (solid line) and Wildenthal's (dashed line) shell-model wave functions with $\Lambda = 1.79$ and $\Lambda = 1.82$, respectively.

for example by Grammaticos³¹ show that the nucleus is soft in the γ direction. The energy versus γ curve for a constrained Hartree-Fock calculation gives a marked triaxially deformed shape for the $K=2$ band, while the curve is very flat for the $K=0$ band; the slightly favored γ is zero or nonzero depending on the force used (especially the spin-orbit force). The transition matrix element is mainly diagonal in γ , and it is clear that, taking into account the zero-point vibration, the result appears similar to that obtained

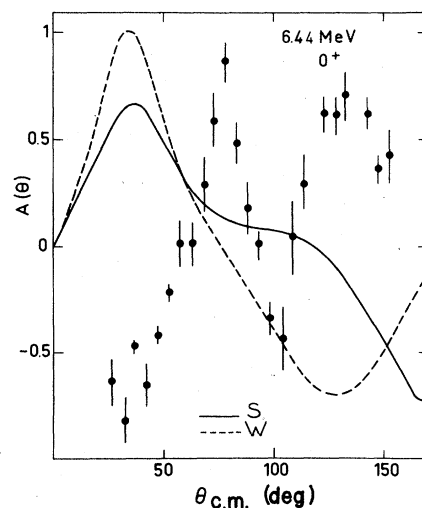


FIG. 23. Same as Fig. 22 for the analyzing powers.

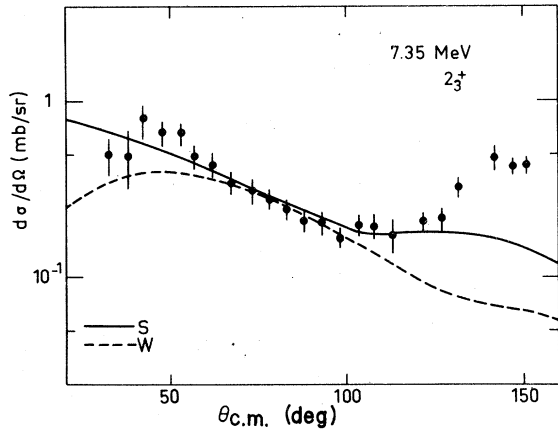


FIG. 24. Experimental and theoretical cross sections for the 2_3^+ state (7.35 MeV) obtained by a DWBA analysis using Soyeur's (solid line) and Wildenthal's (dashed line) shell-model wave functions with $\Lambda = 1.96$ and $\Lambda = 1.48$, respectively.

for a rigid triaxially nucleus with an effective γ , intermediate between the weak minimum energy γ of the $K=0$ band and the strong minimum energy of the $K=2$ band. Thus this effective γ must be considered as a freezing approximation of the γ vibration, as Yamazaki³² also stated.

The microscopic DWBA analysis using shell-model wave functions looks quite disappointing and strongly suggests that important contributions are missing in the calculations. It should be mentioned, however, that due to the use of an effective charge, spin-flip contributions are overestimated compared to the non-spin-flip contributions in the microscopic analysis. It is clear indeed that the use of an effective charge enhances the spin-flip and the non-spin-flip by the same factor, while the enlargement of the configuration space should

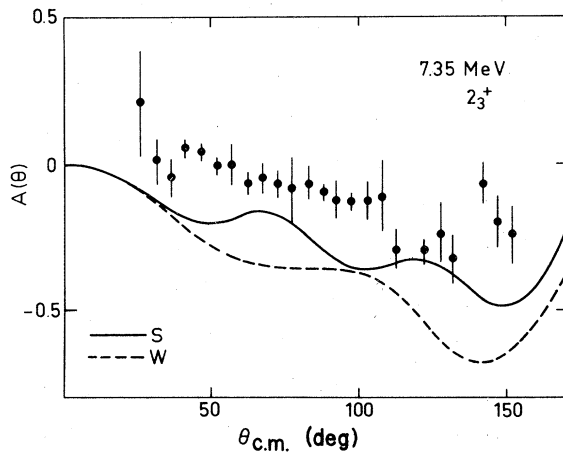


FIG. 25. Same as Fig. 24 for the analyzing powers.

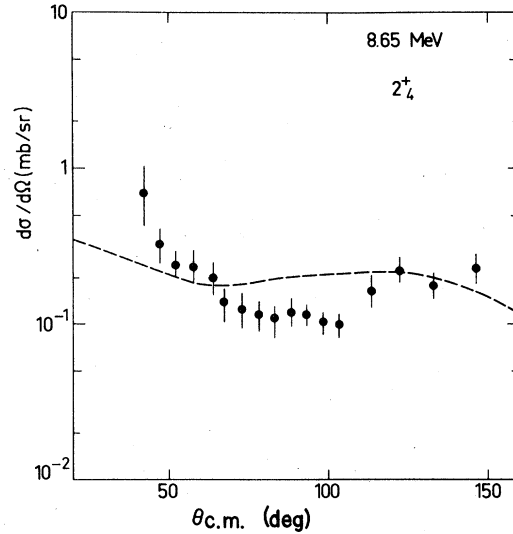


FIG. 26. Experimental and theoretical cross sections for the 2_4^+ state (8.65 MeV) obtained by a DWBA analysis using Wildenthal's shell-model wave function with $\Lambda = 4.47$.

give a much more constructive interference for the non-spin-flip amplitudes than for the spin-flip ones. The collectivity of the model is in fact the constructive interference of the mean contributions added coherently for the non-spin-flip amplitudes. This would explain at the same time the relative success of the macroscopic model and a part of the failure of the microscopic one.

Besides the improvement of the wave functions we can hope to develop the microscopic calcula-

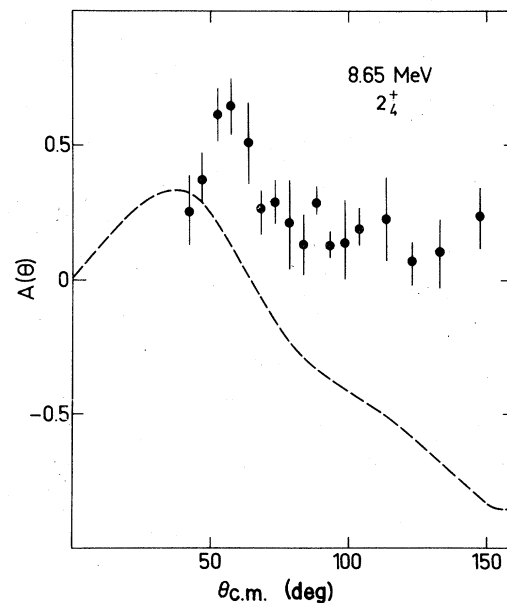


FIG. 27. Same as Fig. 26 for analyzing powers.

tions in two ways:

- (a) An effective interaction realistically derived from the N - N potential, which would include density dependence, energy dependence, and an imaginary part³³;
- (b) the use of a microscopic coupled channel code taking into account the main coupling, in particular the giant resonances.

It is interesting, however, to see how sensitive the analyzing powers and in some cases the cross sections are to very fine details of the nuclear wave functions. This is very clearly demonstrated by our systematic analysis of the data with two

sets of shell-model wave functions calculated in the same valence space and differing only by the effective interaction.

ACKNOWLEDGMENTS

We thank Dr. J. Raynal for his precious help in performing part of the numerical calculations mentioned in this paper. The collaboration of Professor B. H. Wildenthal for the microscopic analyses is gratefully acknowledged. Finally, we would like to thank Professor H. Mc Manus for stimulating comments and very clarifying discussions.

*Present address: Niels Bohr Institute, Blegdamsvej 17, 2100-Copenhagen ϕ , Denmark.

¹M. Soyeur, thesis, Université de Paris-Sud, October 1975 N° A.O.12.151 (unpublished); Ecole de Physique Nucléaire, La Toussuire, February 73, Proceedings S18-1.

²B. H. Wildenthal, private communication.

³A. G. Blair, G. Glashauser, R. de Swiniarski, J. Goudergues, R. M. Lombard, B. Mayer, J. Thirion, and P. Vaganov, Phys. Rev. C 1, 444 (1970); A. B. Plavko, R. M. Lombard, J. Gosset, B. I. Koudrachov, B. Mayer, and J. Thirion, Izv. Akad. Nauk, 38, 878 (1974) [Bull. Acad. Sci. USSR Ser. Fiz. 38, 189 (1974)]; 39, 606 (1975) [39, 120 (1975)]; 40, 828 (1976) [40, 117 (1976)]; 41, 190 (1977) [41, 156 (1977)].

⁴I. Lovas, M. Rogge, U. Schwinn, P. Turek, and D. Ingham, Nucl. Phys. A286, 12 (1977).

⁵G. M. Crawley and G. T. Garvey, Phys. Rev. 160, 981 (1967).

⁶J. Eenmaa, R. K. Cole, C. N. Waddell, H. S. Sandhu, and R. R. Dittman, Nucl. Phys. A218, 125 (1974).

⁷T. Stovall and N. M. Hintz, Phys. Rev. 135, B330 (1964).

⁸M. P. Fricke and G. R. Satchler, Phys. Rev. 139, B567 (1965).

⁹A. A. Rush and N. K. Ganguly, Nucl. Phys. A117, 101 (1968).

¹⁰P. H. Stelson, R. L. Robinson, H. J. Kim, J. Rapaport, and G. R. Satchler, Nucl. Phys. 68, 97 (1965); R. L. Clarke and W. G. Cross, *ibid.* 53, 177 (1964).

¹¹R. J. Griffiths, Nucl. Phys. A102, 329 (1967).

¹²E. Rost, Phys. Rev. 128, 2708 (1962).

¹³E. Colombo, R. Deleo, J. L. Escudié, E. Fabrici, S. Micheletti, M. Pignatelli, and F. Resmini, in Proceedings of the International Conference on Nuclear Structure, Tokyo, 1977, edited by T. Marumori. [J. Phys. Soc. Jpn. Suppl. 44, 543 (1978)]; M. Pignatelli, in Proceeding of the European Physical Society Meeting, Firenze, 1977 (unpublished).

¹⁴J. L. Escudié, R. Lombard, M. Pignatelli, F. Resmini, and A. Tarrats, Phys. Rev. C 10, 1645 (1974).

¹⁵J. Borysowicz, H. Mc Manus, and G. Bertsch (unpub-

lished).

¹⁶F. Resmini, J. L. Escudié, M. Pignatelli, J. Gosset, A. Tarrats, and E. Fabrici, Phys. Rev. C (to be published).

¹⁷S. Kahana, H. C. Lee, and C. K. Scott, Phys. Rev. 185, 1378 (1969); H. C. Lee, private communication.

¹⁸W. Chung, thesis, Michigan State University, 1976 (unpublished); W. Chung and B. H. Wildenthal, private communication.

¹⁹D. Branford, A. C. Mc Gough, and I. F. Wright, Nucl. Phys. A241, 349 (1975).

²⁰F. Leicca, thesis, Université de Bordeaux, 1973 (unpublished).

²¹Y. Terrien, J. L. Escudié, B. Buenerd, J. M. Loiseaux, P. Martin, and J. B. Viano, Phys. Lett. 45B, 235 (1973).

²²G. R. Satchler, Phys. Lett. 35B, 279 (1971); Z. Phys. 260, 209 (1973).

²³J. Raynal, Report No. IAEA-SMR-8/8, 1972 (unpublished).

²⁴R. de Swiniarski, C. Glashauser, D. L. Hendrie, J. Sherman, A. D. Bacher, and E. A. Mc Clatchie, Phys. Rev. Lett. 23, 317 (1969).

²⁵H. R. E. Tjin, A. Djie, K. Mulder, F. Udo, A. Groeneveld, L. A. Ch.Koerts, A. D. Hill, and P. E. Hodgson, Nucl. Phys. A106, 85 (1968).

²⁶K. A. Eberhard and D. Robson, Phys. Rev. C 3, 149 (1971); K. A. Eberhard and G. Mayer-Böricke, Nucl. Phys. A142, 113 (1970).

²⁷T. Tamura, Nucl. Phys. 73, 241 (1965); J. Kokame, K. Fukunaga, N. Inoue, and H. Nakamura, Phys. Lett. 8, 342 (1964).

²⁸H. Rebel, G. W. Schweimer, G. Schatz, J. Specht, R. Löhken, G. Hauser, D. Habs, and H. Klewe-Nebenius, Nucl. Phys. A182, 145 (1972).

²⁹R. Helm, Phys. Rev. 104, 1466 (1956).

³⁰Y. Horikawa, Y. Torizuka, A. Nakada, S. Mitsunobu, Y. Kojima, and M. Kimura, Phys. Lett. 36B, 9 (1971).

³¹B. Grammaticos, Nucl. Phys. A252, 90 (1975).

³²T. Yamazaki, Nucl. Phys. 49, 1 (1963).

³³F. A. Brieva and J. R. Rook, Nucl. Phys. A291, 299 (1977); A291, 317 (1977); A297, 206 (1978).